

Reduction of group delay ripple of multi-channel chirped fiber gratings using adiabatic UV correction

P. I. Reyes, M. Sumetsky, N. M. Litchinitser*, and P. S. Westbrook

*OFS Laboratories, 600 Mountain Ave., Murray Hill, NJ 07974, USA
preyes@ofsoptics.com, sumetski@ofsoptics.com, westbrook@ofsoptics.com*

**OFS Laboratories, 19 Schoolhouse Road, Somerset, NJ 08873, USA
natashal@ofsoptics.com*

Abstract: We demonstrate reduction of group delay ripple (GDR) from 24 ps to 9 ps peak to peak in a four channel 43 Gb/s dispersion compensating chirped fiber grating by adiabatic UV post processing. The eye opening penalty due to the grating GDR was improved from ~2dB to <1dB for all of the channels over a range of carrier frequencies of 15GHz. Our results demonstrate that at 43 Gb/s, the adiabatic UV correction technique is sufficient to substantially improve multi-channel fiber grating performance. We also discuss three limitations of the correction technique which cause GDR to vary from channel to channel: Noise in the sampling function, cladding mode loss, and varying channel reflectivity. While these limitations are visible in our results they do not reduce the effectiveness of the adiabatic correction for our gratings.

©2004 Optical Society of America

OCIS codes: 060.0060 Fiber optics and optical communications; (060.2330) Fiber optics communications; (060.2340) Fiber optics components; (230.1480) Bragg reflectors; (230.1950) Diffraction gratings

References and links

1. D. J. Moss, S. McLaughlin, G. Randall, M. Lamont, M. Ardekani, P. Colbourne, "Multichannel tunable dispersion compensation using all-pass multicavity etalons," OFC 2002 Technical Digest (Optical Society of America, Washington, D.C.), 132.
2. C. K. Madsen, "Integrated waveguide all pass filter tunable dispersion compensators," OFC 2002 Technical Digest (Optical Society of America, Washington, D.C.), 131.
3. Y. Li, B. Zhu, C. Soccolich, L. Nelson, N. Litchinitser, G. Hancsin, "Multi-Channel High-Performance Tunable Dispersion Compensator For 40 Gb/s Transmission Systems," OFC 2003 Technical Digest 2, (Optical Society of America, Washington, D.C.), 517.
4. W. H. Loh, F. Q. Zhou, and J. J. Pan, "Sampled Fiber Grating Based-Dispersion Slope Compensator," IEEE Phot. Tech. Lett. **11**, 1280, October 1999.
5. H. Li, Y. Sheng, Y. Li, and J. E. Rothenberg, "Phased-Only Sampled Fiber Bragg Gratings for High-Channel-Count Chromatic Dispersion Compensation," J. Lightwave Technol. **21**, 2073-2084 (2003).
6. A. K. Ahuja, P. E. Steinvurzel, B. J. Eggleton, J. A. Rogers, "Tunable single phase-shifted and superstructure gratings using microfabricated on-fiber thin film heaters," Opt. Commun. **184**, 119-125, October 2000.
7. R. Lachance, S. Lelièvre, Y. Painchaud, "50 and 100GHz Multi-Channel Tunable Chromatic Dispersion Slope Compensator," OFC 2003 Technical Digest 1, (Optical Society of America, Washington, D.C.), 164.
8. B. J. Eggleton, A. Ahuja, P. S. Westbrook, J. A. Rogers, P. Kuo, T. N. Nielsen, and B. Mikkelsen, "Integrated tunable fiber gratings for dispersion management in high-bit rate systems," J. Lightwave Technol. **18**, 1418-1432 (2000)
9. A. V. Buryak and D. Y. Stepanov, "Correction of systematic errors in the fabrication of fiber Bragg gratings," Opt. Lett. **27**, 1099 (2002).
10. T. Komukai, T. Inui, M. Kurihara, S. Fujimoto, "Group-delay ripple reduction in step-chirped fiber Bragg gratings by using laser-beam written step-chirped phase masks," IEEE Photon. Technol. Lett. **14**, 1554-1556 (2002).

11. K. Y. Kolossovski, R. A. Sammut, A.V. Buryak, D. Y. Stepanov, "Three-step design optimization for multi-channel fibre Bragg gratings," *Opt. Express* **11**, 1029-1038 (2003).
<http://www.opticsexpress.org/abstract.cfm?URI=OPEX-11-9-1029>
12. M. Sumetsky, P. I. Reyes, P. S. Westbrook, N. M. Litchinitser, and B. J. Eggleton, "Group delay ripple correction in chirped fiber Bragg gratings," *Opt. Lett.* **28**, 777-779, (2003).
13. M. Sumetsky, P. S. Westbrook, P. I. Reyes, N. M. Litchinitser, B. J. Eggleton, Y. Li, R. Deshmukh, C. Socolich, F. Rosca, J. Bennike, F. Liu, and S. Dey, "Reduction of chirped fiber grating group delay ripple penalty through UV post processing," *Optical Fiber Communication Conference Postdeadline Papers PD28-1*, OSA, Washington DC, 2003.
14. N. M. Litchinitser, Y. Li, M. Sumetsky, P. S. Westbrook, and B. J. Eggleton, "Tunable dispersion compensation devices: Group delay ripple and system performance," in *OSA Trends in Optics and Photonics (TOPS)*, **86** Optical Fiber Communication Conference 2003, Technical Digest, Postconference Ed. (Optical Society of America, Washington, D. C., 2003) pp. 163-164.
15. M. Sumetsky, B. J. Eggleton, C. M. de Sterke, "Theory of group delay ripple generated by chirped fiber gratings," *Opt. Express* **10**, 332-340 (2002),
<http://www.opticsexpress.org/abstract.cfm?URI=OPEX-10-7-332>
16. M. Sumetsky, N. M. Litchinitser, P. S. Westbrook, P. I. Reyes, B. J. Eggleton, Y. Li, R. Deshmukh, C. Socolich, F. Rosca, J. Bennike, F. Liu, S. Dey "High-performance 40 Gbit/s fibre Bragg grating tunable dispersion compensator fabricated using group delay ripple correction technique," *Electron. Lett.* **39**, 1196-1198, Aug. 7, 2003.

1. Introduction

The development of multi-channel dispersion compensation (MDC) devices is of significant interest due to their use in single channel applications requiring "colorless" or broadband components that are valid for many channels over a large range of wavelengths, as well as applications requiring operation for multiple channels simultaneously. Recent examples include multi-cavity etalons [1], waveguide all-pass filters [2], chirped superstructure fiber Bragg gratings (CSFBG) [3], CSFBGs using interleaving [4] and MDCs from binary and multilevel phase only sampling methods [5]. Tunable MDCs have also been demonstrated [6,7]. One of the most serious limiting factors in the performance of MDC devices has been group delay ripple (GDR). A large GDR value can give rise to substantial OSNR penalty [8]. The GDR in CSFBGs is caused by both random and systematic errors in the grating writing process. Several works have been done in the correction of GDR in fiber Bragg gratings as well as optimization of the fabrication process to minimize the GDR [9-11]. We have recently demonstrated reduction of GDR of single channel linearly chirped fiber Bragg gratings by iterative UV post processing correction [12,13]. For CSFBGs, the GDR reduction is even more critical because these gratings require stronger UV-induced index change, and GDR grows with increased UV-induced index. Moreover, as we discuss below, it is expected that in superstructure gratings, the corrective profile derived from a single channel may be applicable to all of the channels, making UV correction a useful tool for such CSFBGs just as it is for single channel gratings.

In this paper, we demonstrate correction of the low frequency GDR of CSFBGs using UV post-processing and the slowly varying or adiabatic GDR [12,13]. In our work we consider only the effect of "DC index" corrections that change the local Bragg condition (through DC UV exposure), however AC index changes may also be considered in the slowly varying limit. In the adiabatic regime the GDR is directly proportional to the DC index correction profile. This condition is valid when the DC index variations occur on length scales longer than the distance over which the incident and reflected waves vary at the resonant part of the grating. We show that for applications at 43 Gb/s this method can significantly reduce the low frequency GDR for all channels of a multichannel grating. We also show that the resulting eye opening penalty (EOP) due to the grating GDR (a measure of the quality of the grating's performance indicating its ability to compress pulses and not introduce an additional penalty due to GDR [14]) is also improved substantially (from 1 to 0.5dB). The effectiveness of the adiabatic approximation for our 43Gbit/s gratings is aided by the convergence of two characteristic wavelength scales in our gratings: The adiabatic correction wavelength range, which is >0.1 nm in our gratings [14,15]; and the wavelength scale that affects system penalty

at >43 Gb/s (a few tenths of a nm) [14]. These wavelength scales depend on the grating chirp (dispersion) and strength, and on the bit rate (pulse width), and therefore adiabatic correction algorithms will have varying degrees of effectiveness depending on the grating and pulse parameters.

While the limitations of the adiabatic approximation in single channel gratings have been described elsewhere [12,13], in this work we discuss the limitations of applying UV post processing to multichannel gratings. The fundamental problem with multichannel correction is that the GDR may vary from one channel to the next, complicating the determination of a corrective profile, especially in the adiabatic regime which explicitly assumes that all channels will have the same GDR. We identify three sources of variation of the GDR from channel to channel: noise in the superstructure period, cladding mode resonances, and variation in channel reflectivity. While none of these mechanisms is limiting in our application, our results show the effect that they have on the applicability of adiabatic and other GDR correction schemes.

2. GDR in multi-channel gratings

The reproducibility of GDR for all channels is critical for the application of multi-channel grating correction. To examine the origins of GDR in multi-channel gratings we consider the simplest example of a two-channel grating:

$$\begin{aligned} \Delta n_{ac}(z) &= \Delta n_0 \left[\sin(k_1 z + Cz^2 + \varphi_1(z)) + \sin(k_2 z + Cz^2 + \varphi_2(z)) \right] \\ &= \Delta n_0 \sin\left(\frac{k_1 + k_2}{2} z + Cz^2 + \frac{\varphi_1(z) + \varphi_2(z)}{2}\right) \cos\left(\frac{k_1 - k_2}{2} z + \frac{\varphi_1(z) - \varphi_2(z)}{2}\right) \end{aligned} \quad (1)$$

The first line of Eq. (1) corresponds to the AC index $\Delta n_{ac}(z)$ of two single channel gratings having channel separation $k_1 - k_2$. Here the coefficient C determines the chirp of the gratings and functions $\varphi_1(z)$ and $\varphi_2(z)$ determine the spatial phase noise at each exposure. We ignore amplitude noise in this simplified analysis. Clearly, the two phase terms are in general independent and a corrective profile derived from one of the channels will not be applicable to the other channel. The second line of Eq. (1) corresponds to the AC index introduced by a single exposure through a sinusoidal amplitude modulated phase mask. In this case the spatial noise is separated into the noise in the high-frequency AC index modulation $\varphi_{\text{Bragg}}(z) = (\varphi_1(z) + \varphi_2(z))/2$, and noise in the low-frequency superstructure period variation, $\varphi_{\text{superstructure}}(z) = (\varphi_1(z) - \varphi_2(z))/2$. In this case, provided that $\varphi_{\text{superstructure}}(z)$ is small, each channel will see the same high frequency phase noise, $\varphi_{\text{Bragg}}(z)$, and grating correction derived from one channel will be applicable for both channels. Therefore, just as phase noise in the grating period causes GDR in the single channel grating, phase noise in the superstructure period will cause channel-to-channel variations of GDR. This effect may also be understood with a simple Fourier argument: The noise in the superstructure period may be understood as the addition of Fourier components to the superstructure that are not simply multiples of the fundamental superstructure period $(k_1 - k_2)/2$. Such superstructure Fourier components would have the effect of generating grating GDR with a different wavelength spacing from that of the fundamental superstructure period. This “aperiodic” grating GDR will be roughly added to the fundamental periodic grating response, thus resulting in an overall grating response that is different for each channel. Note that this argument employs Fourier components and superstructure side bands similar to the GDR cutoff arguments described in [15].

However, even if the grating has a single superstructure period, there are other sources of noise that can make each channel profile different from another. In particular, the presence of cladding mode loss, which occurs on the short wavelength side of a fiber Bragg resonance, can cause the superstructure grating response to vary from channel to channel. This can be most easily understood by considering the longest wavelength resonance of a multi-channel fiber Bragg grating, which will not overlap with any cladding mode resonances from the other channels, unlike the shortest wavelength resonance, which will coincide with the cladding

mode resonances from all of the longer wavelength channels. While not large in our experiment, we show the effect of cladding modes in our results.

Another source of channel irreproducibility originates from differences in channel reflectivities. As we discuss later, the strong channels display mostly phase ripple, and very little amplitude ripple, whereas for weak channels, amplitude ripple is more pronounced and affects the channel's response to the correction. While our results exhibit these effects, they are not pronounced, and do not affect the usefulness of the adiabatic correction at 43Gbit/s.

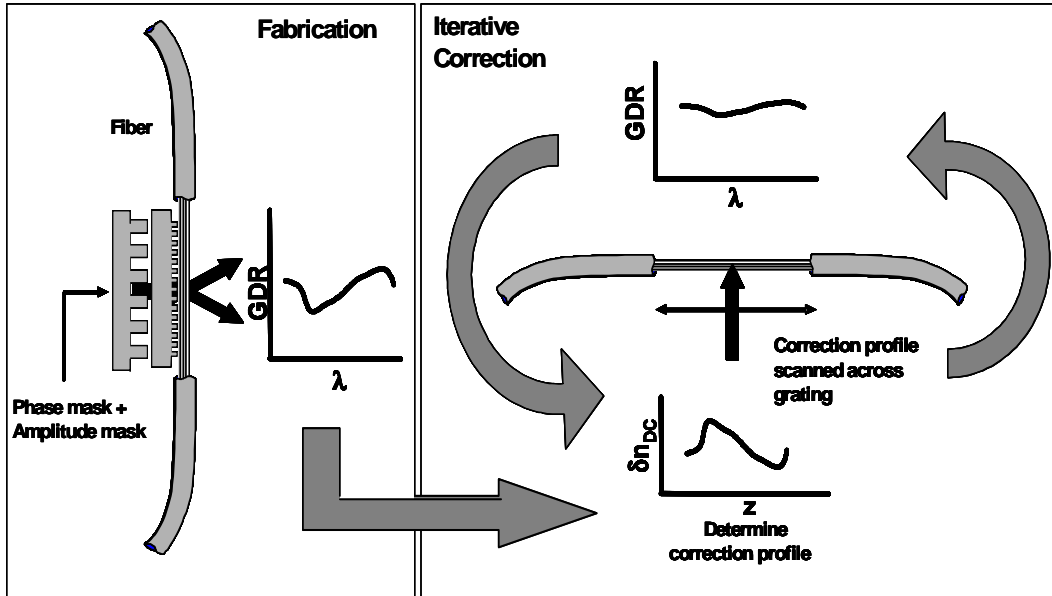


Fig. 1. Experimental setup used to fabricate the multi-channel gratings and implement the iterative correction method.

3. CSFBG correction

The superstructure grating we used for the GDR correction is 8 cm-long and is written using the experimental apodization function defined by Eq. (2)

$$n(z) = A \exp \left\{ -\alpha \exp \left(\beta \ln \left(\frac{(z-z_0)^2}{d^2} \right) \right) \right\} \quad (2)$$

where: $\alpha = 10$, $\beta = 5$, and $d = 80$ mm. The grating is also linearly chirped with a mask chirp rate of 0.094 nm/cm. The grating is written by scanned UV exposure (248nm excimer laser; gaussian beam width ~1cm) through a dielectric-coated amplitude mask placed behind the phase mask. The amplitude mask period is 0.347 mm with 35% duty cycle. The resulting grating has four strong channels exceeding 95% reflection before annealing. The design of such a grating is meant for “colorless” single channel tunable DC applications, thus the channel spacing is large compared to typical channel spacing and the dispersion is relatively low [3]. After the superstructure grating is written, its per channel GDR is measured using the Agilent 86037C Dispersion Test Set with 2.5pm wavelength steps. The GDR of each channel is then averaged within a 0.1nm window. The smoothed GDR profile features repeat themselves for each channel with slight variations (see Fig. 4). The smoothed GDR is then averaged over channels to arrive at the GDR profile which is used to create a corrective DC index profile $\Delta n_{correction}(z)$ by performing the simple adiabatic rescaling $\Delta n_{correction}(z) = A \Delta \tau(k(\lambda - \lambda_0))$ described in [12,13] which primarily consists of determining the correct index amplitude A , chirp rate k , and wavelength offset λ_0 , where $\Delta \tau$ is

the smoothed GDR averaged over all channels. Introducing the corrective DC profile to the grating trims all the channels simultaneously. The process is performed iteratively until substantial GDR reduction is achieved. Figure 1 shows the experimental setup we used to fabricate the multi-channel grating and implement the iterative correction method.

To determine the adiabatic rescaling parameters correctly for each iteration we use the observed GD change for a given correction. We performed this calibration on the corrective DC index profile by taking the difference of the grating's GDR before and after a correction profile has been applied. We smoothed the difference by 0.1 nm and compared it to the applied correction profile. For a perfect correction the two curves should match, otherwise the adiabatic rescaling parameters should be changed accordingly in the next iteration. Figure 2 illustrates this procedure. On the top plot, the solid heavy black curve is the observed GDR of one of the channels of the multi-channel grating, while the thin solid gray curve represents the GDR after a correction profile (heavy dashed black curve at the bottom plot; this was the observed GDR averaged over 0.1nm and rescaled) has been applied. The difference of the two GDR's is then smoothed by 0.1 nm to obtain the observed differential (thin dotted black curve at the bottom plot). The parameters used to generate the correction profile are correct if the observed differential matches the applied correction profile as shown in this case.

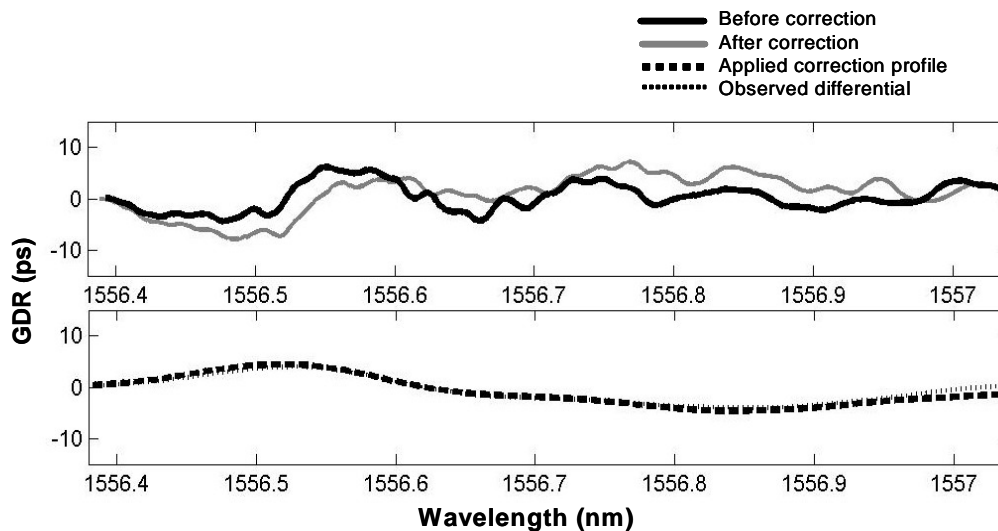


Fig. 2. Calibration of the adiabatic rescaling parameters to create an accurate correction profile. If the observed differential matches the applied correction profile, then the rescaling parameters A , k , and λ are correct.

The total UV correction profile for all iterations should be consistent with the differential of the initial and final GDRs. Figure 3 shows the GDRs for the initial and final iteration (top plot) of one of the channels of the grating together with the total applied correction profile (bottom plot in heavy dashed lines) and the differential curve (bottom dotted curve). Note that after rescaling the total corrective dosage vs. position profile using the parameters in the correction algorithm, we see that the total correction profile matches fairly well the differential between initial and final iteration GDRs.

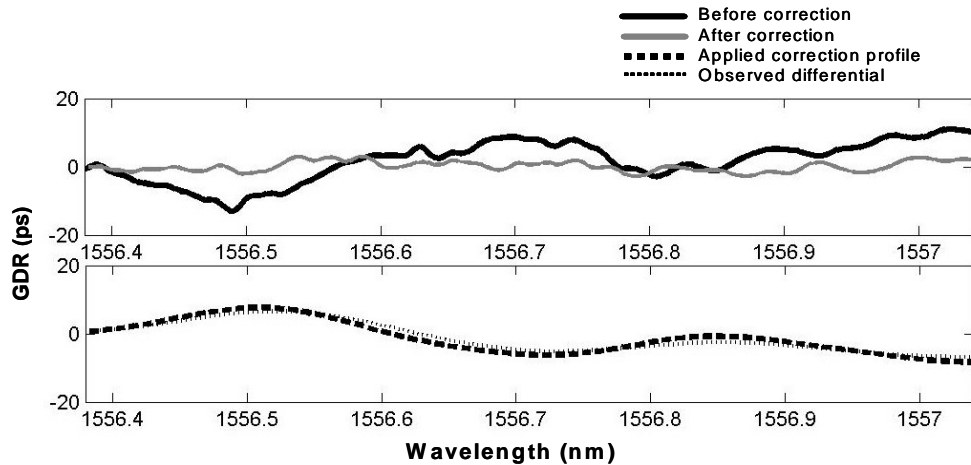


Fig. 3. The total applied correction profile matches the differential between the GDRs of the initial and final iterations.

In Fig. 4, we show the results of correction for four channels of the superstructure grating. The per-channel GDRs averaged over 0.1 nm are plotted before correction (top, black), after correction (middle, green), and also after an anneal at 120°C for 12 hours (bottom, red). Note that an arbitrary offset was added in x and y to the three reflection and GDR plots (black, green, and red) from each channel to simplify the comparison. The reference level for the reflection spectra in black is 0dB, -1 dB for the green plot, and -2 dB for the red plot. Also note that the grating is measured in-situ after inscription as well as during the iterative correction process, whereas after annealing it is measured after being re-mounted and respliced. Therefore the reference levels of the grating's reflection spectrum before and after annealing are different. Thus, one cannot accurately deduce the effect of annealing simply from comparing the amplitude of the reflection spectrum before and after anneal. However, one can conclude that the grating has weakened as expected after anneal by noting the reduction in bandwidth of the reflection spectrum for each channel of the grating after anneal. A quantitative measure of the change in reflectivity could be obtained from transmission measurements before and after anneal, but these were not part of our experimental setup, since their quantitative measure was not needed to obtain a measure of the GDR stability. Figure 4 shows that the GDR peak to peak value has been reduced from 24 ps to 9 ps. Note that remounting of the grating after anneal could result in polarization fluctuations of a few ps in the anneal GDR value. Comparison of the corrected GDR before and after annealing demonstrates acceptable thermal stability of our correction technique within our given annealing conditions. A full study of the thermal stability under various annealing and writing conditions is beyond the scope of this work, and our annealed data is recorded here as a proof of principle demonstration of the thermal stability of the correction process.

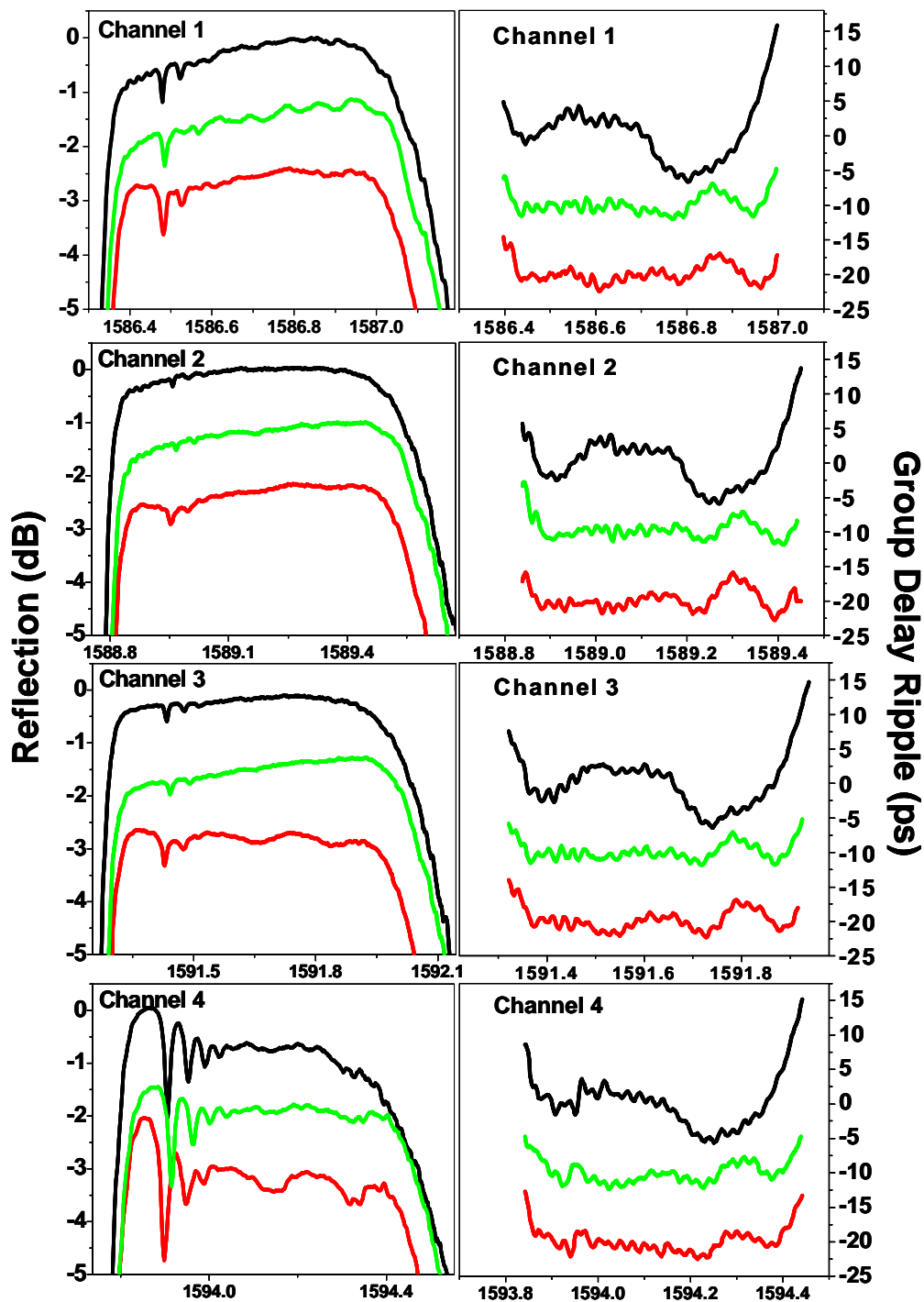


Fig. 4. Plots of reflection spectrum (left row) and smoothed GDR (right row) of the four channels of the superstructure grating. In each channel plot, black: before correction, green: after correction, red: after anneal. Note that an arbitrary offset was added in x and y to the three reflection and GDR plots (black, green, and red) from each channel to simplify the comparison. The reference level for the reflection spectra in black is 0dB, -1 dB for the green plot, and -2 dB for the red plot.

The GDR of the grating is a convenient characteristic of the device's performance, but a more relevant quantity is the eye-opening penalty (EOP) [14]. To measure this quantity we represent the measured grating response as

$$R = r \exp [\alpha + \alpha_{\text{noise}}(\omega) + i\phi_{\text{noise}}(\omega)] \quad (3)$$

where $r \exp(\alpha)$ is the reflectivity of the grating, $\alpha_{\text{noise}}(\omega)$ is the amplitude noise due to the ripple in the reflectivity, and $\phi_{\text{noise}}(\omega)$ is the phase noise due to the GDR. Our simulation setup to calculate the EOP due to the FBG consists of a 43Gb/s NRZ transmitter, the multichannel FBG characterized by its amplitude response versus wavelength and phase ripple versus wavelength (Eq. 3), and a receiver. The amplitude response of the FBG was taken directly from the measurement data. To find ϕ_{noise} we first chose the center wavelength for the EOP simulations λ_{center} as 0.05nm higher than the center of the reflection bandwidth. To find the phase ripple, we make a linear fit to the measured group delay in an interval ranging from 0.3nm above and below λ_{center} . The linear fit is then subtracted from the original group delay to obtain the group delay ripple. Note, that the slope of group delay determines the dispersion of the grating, therefore by subtracting a linear fit from a measured group delay we assume that the grating ideally compensates for a certain amount of dispersion (given by the slope of this linear fit), and the remaining ripple causes the EOP. Finally we integrate the resulting group delay ripple to get the phase ripple that is used in the simulation, $\phi_{\text{noise}}(\omega)$. To simplify the calculations, we assume that the phase ripple outside the wavelength interval $[\lambda_{\text{center}}-0.3\text{nm}, \lambda_{\text{center}}+0.3\text{nm}]$ is zero. Note, that although we present EOP calculated for carrier frequency offsets from approximately -35GHz to $+35\text{GHz}$ in Figs. 6, 7 and 8, in real systems we are interested in smaller offset drifts ($\sim \pm 10\text{GHz}$), and this assumption does not affect the EOP in these smaller ranges. In this work we consider EOP improvements over only a 15GHz range at the band center. Similar treatment of EOP showed quantitative agreement with experimentally measured optical signal-to-noise ratio (OSNR) penalty [16]. We modeled the receiver as an idealized photodiode (with responsivity of 1A/W , infinite bandwidth, no thermal or shot noise, and no dark current) followed by a fifth order electrical Bessel filter. The eye opening of the signal at the output of the electrical filter is measured as the height of the tallest rectangle (with a fixed width of 20% of the bit period) that can be fitted into the eye divided by the average optical power incident on the photodiode. The eye opening penalty (EOP) is computed as the ratio between the eye opening with and without the FBG.

Figure 5 illustrates our definition of EOP. Shown in this figure are the 43 Gb/s NRZ eye diagrams for the signals after the electrical Bessel Filter without the grating (left plot), and with the grating (right plot). Rectangles of fixed width (20% of the bit period) are fitted within each eye diagram by adjusting their heights. The EOP due to the grating GDR can be conceptually described as the reduction of the height of the rectangle from the eye diagrams with the grating compared to the height of the rectangle from the eye diagram without the grating. The EOP is computed first for amplitude-only effects, second for phase-only effects - and lastly, for both amplitude and phase effects present. If we only take into account the effects of the multi-channel dispersion compensator into the system then the OSNR penalty due to the device is roughly twice the EOP. In the simulations the EOP is computed based on the eye diagram after the electrical filter instead of just from the grating [14].

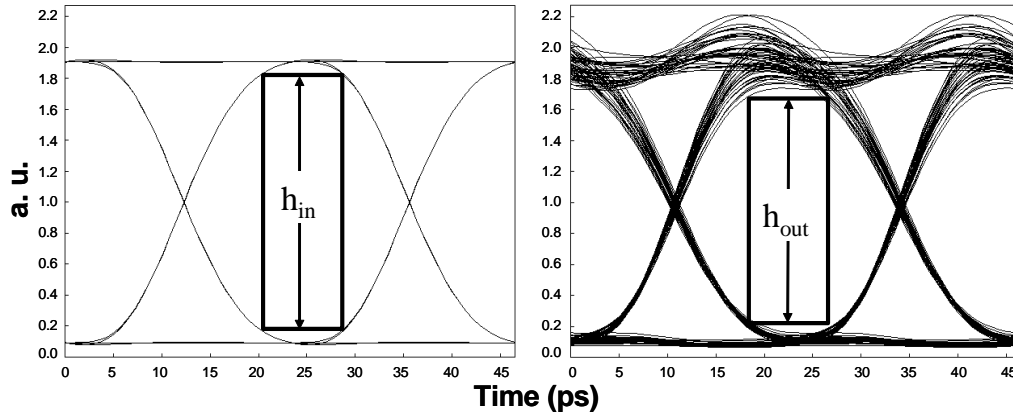


Fig 5. 43 Gb/s NRZ eye diagrams at the output of the electrical Bessel filter of the simulation setup without the grating (left plot) and with the grating (right plot). Rectangles of fixed widths (20% of the bit period) are fitted within each eye diagram by adjusting their heights. The reduction in height gives a measure of the EOP.

Figure 6 shows simulation plots of the 43Gbit/s NRZ EOP of each channel before and after grating correction. We have demonstrated that after correction the EOP due to the superstructure grating have been reduced from ~ 2 dB to < 1 dB over a range of ~ 15 GHz of carrier frequency tuning near the band center. These plots show the EOP due to only the phase noise, only the amplitude noise, and both noises together. We note that the phase noise contribution is dominant, and that our correction technique reduces the EOP from the phase noise while leaving the contribution from the amplitude noise small. This is to be expected, since the reflectivity is large and thus insensitive to variations in the local Bragg wavelength, and moreover, the data used in generating the corrective profiles was derived from the GDR.

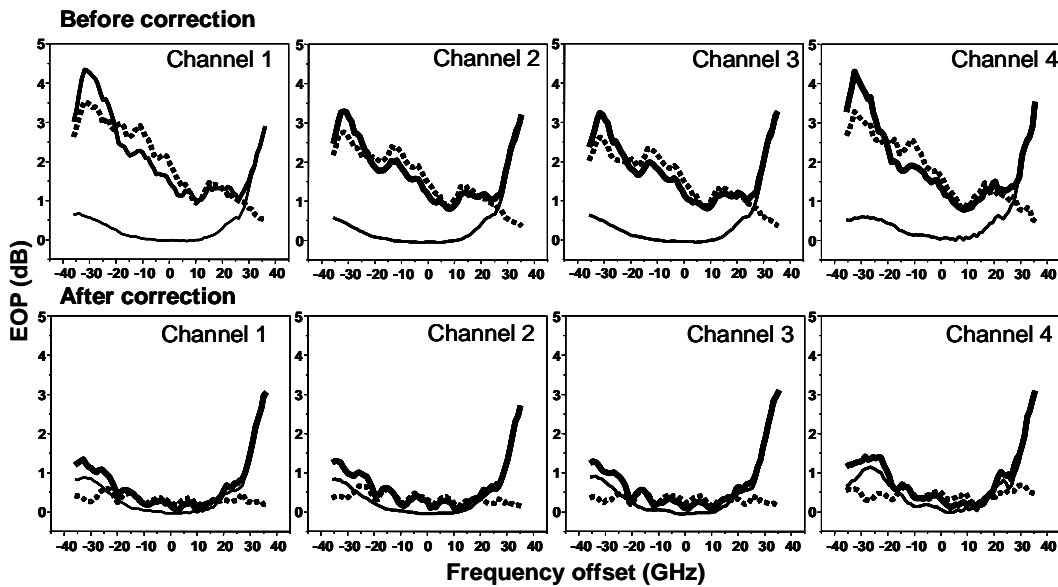


Fig. 6. EOP simulation plots for the four strongest channels before and after correction of the superstructure grating GDR. Zero detuning corresponds to approximate center of the reflection band of Fig. 4. Solid: amplitude, dashed: phase, bold: both. EOP near zero frequency offset improves by 0.5 to 1 dB in all channels.

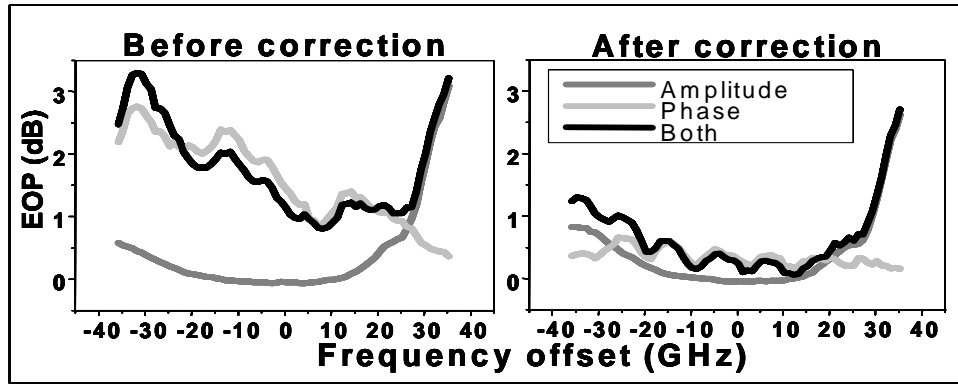
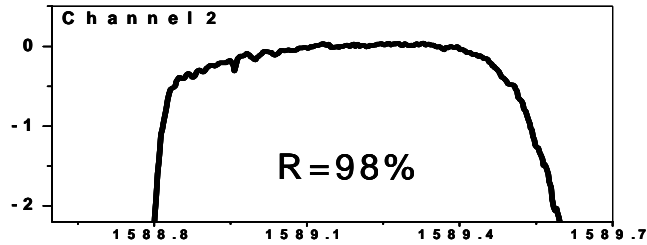
However, if channels are weak, the effect of the amplitude ripple on the correction of the grating becomes significant. To illustrate this point we reproduce in Fig. 7 the EOP plots for channels 2 and 4 before and after correction. Channel 2 represents a strong channel (~98% reflectivity), while channel 4 represents a weak channel (~80% reflectivity). Note that the amplitude ripple is noticeably larger in the weak channel. For a strong channel we would observe that after correction the EOP due to amplitude-only effects does not change significantly hence the overall EOP improvement results from correction of the phase noise. On the other hand, notice that the profile of the EOP due to the amplitude-only effects changes significantly after correction in a weak channel which can be seen in Fig 7 encircled in red. In this case the overall EOP features contain not only the changes due to the phase-only effects but also from the amplitude ripple. Note that even though we can observe the effect of the amplitude ripple on the correction in weak channels, the effect is not large enough to greatly affect the overall improvement of the EOP after correction.

Another limitation to multi-channel correction is the presence of cladding mode loss in the grating. It was mentioned earlier that the cladding mode loss in the grating introduces asymmetry to the channels. This asymmetry is illustrated in Fig. 8. The boxed area of the transmission spectrum of the multi-channel grating shows the cladding mode loss. This can be removed by coating the grating with index-matching material. However, during the correction procedure the grating is not index-matched so the effect of the cladding mode loss is included in the corrective profiles. The effect of not removing the cladding mode loss can either improve or worsen the correction of the grating. To show this we immersed the grating in index-matching oil after the correction and annealing were performed. The EOP plots for two of the channels of the multi-channel grating in Fig. 8 shows the effect of index matching the grating. The changes in the EOP after index matching, although not large in our experiment, shows the different responses of each channel to the removal of the cladding mode effects. Note that the EOP of the channel corresponding to the longest wavelength resonance (channel 4) does not significantly change after index matching, while the EOP of the shorter wavelength channel (channel 1) is noticeably changed after index matching as can be seen in the 0.5 dB increase of the EOP at the -10 GHz frequency offset locations. This shows that the channel corresponding to the longest wavelength resonance is less affected by the cladding mode asymmetry because it does not overlap with the cladding mode resonances while the shorter wavelength channels are affected more since they overlap with the cladding mode resonances.

Note that thermal tuning applications typically require an uncoated fiber to allow for larger temperature variations, therefore the correction applied to the uncoated fiber during grating fabrication yields the desired result for the final tunable device. Moreover, cladding mode loss may be reduced with optimized fibers and by reducing the strength of the fiber grating.

Finally we note that very small changes in GDR may arise due to grating polarization dependence. Birefringence due to native fiber asymmetry and UV irradiation will cause the grating response to split into two polarization dependent responses. This polarization dependence is assumed to be small in our case. The differential group delay (DGD) of our gratings was typically a few ps or less, therefore this would have been the maximum error observable in the corrective profile. Such a shift in GDR would only be observed if there was a substantial change in the polarization (180 degrees on the Poincare sphere). The fibers and measurements were stable enough in our measurements that polarization dependence could be ignored.

**Strong
Channel**



**Weak
Channel**

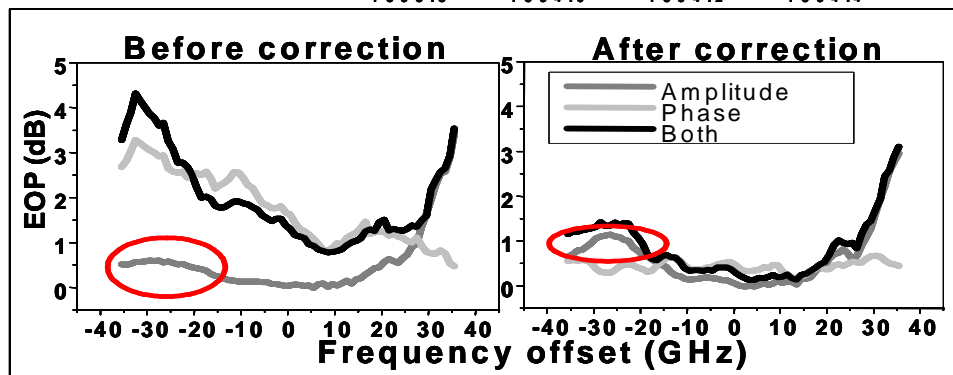
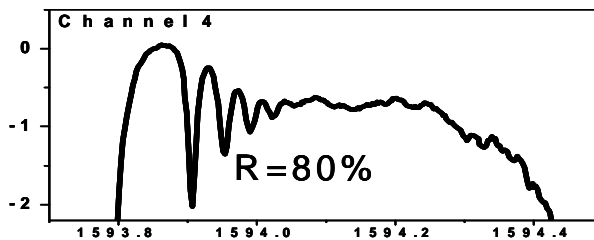


Fig. 7. Amplitude ripple affects the overall EOP of the grating for weak channels after correction. Notice that for the weak channel the EOP due to amplitude only effects already exhibits a small change after the correction has been applied (dark gray plot encircled in red).

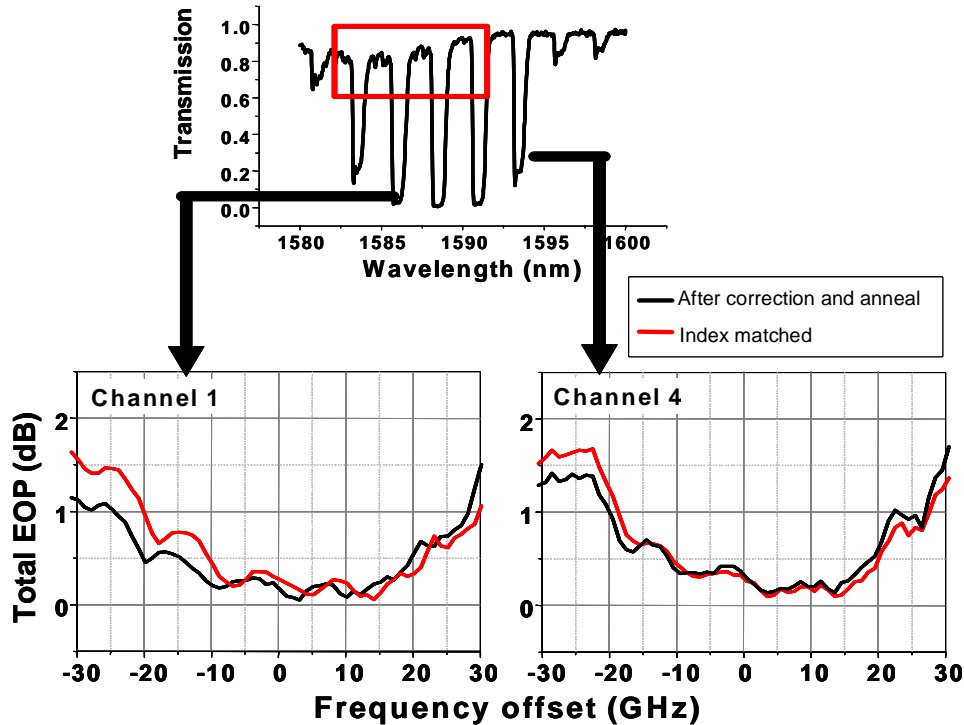


Fig. 8. Cladding mode loss introduces asymmetry to the multi-channel grating making the channel responses vary. The grating was index matched after the correction process to see the effect of changing the cladding mode loss. The EOPs of two of the channels show effect of cladding mode loss on GDR.

Conclusion

We have demonstrated that adiabatic UV post processing correction of GDR may be applied to a multi-channel chirped fiber grating fabricated with amplitude sampling. The low-frequency GDR was reduced from 24 ps to 9 ps peak to peak and the corresponding NRZ 43Gbit/s EOP from ~2dB to <1 dB in a 15GHz range of carrier frequency. We have also examined some of the limitations of multichannel grating correction algorithms. The limitations include noise in the sampling period, cladding mode loss, and variations in channel strengths. While we are able to observe these limitations in our application, they are not large enough to compromise the effectiveness of the adiabatic corrections.